

Constraining new physics with searches for long-lived particles: Implementation into SModelS

Jan Heisig^a, Sabine Kraml^b, Andre Lessa^c

^a*Institute for Theoretical Particle Physics and Cosmology, RWTH Aachen University, 52056 Aachen, Germany*

^b*Laboratoire de Physique Subatomique et de Cosmologie, Université Grenoble-Alpes, CNRS/IN2P3,
53 Avenue des Martyrs, F-38026 Grenoble, France*

^c*Centro de Ciências Naturais e Humanas, Universidade Federal do ABC, Santo André, 09210-580 SP, Brazil*

Abstract

We present the implementation of heavy stable charge particle (HSCP) and R -hadron signatures into SModelS v1.2. We include simplified-model results from the 8 and 13 TeV LHC and demonstrate their impact on two new physics scenarios motivated by dark matter: the inert doublet model and a gravitino dark matter scenario. For the former, we find sensitivity up to dark matter masses of 580 GeV for small mass splittings within the inert doublet, while missing energy searches are not able to constrain any significant part of the cosmologically preferred parameter space. For the gravitino dark matter scenario, we show that both HSCP and R -hadron searches provide important limits, allowing to constrain the viable range of the reheating temperature.

1. Introduction

Exploring physics beyond the standard model (BSM) is one of the key scientific goals of the LHC. Simplified models have turned out to provide useful benchmarks for interpreting LHC results and investigating their implications for the open questions of today's fundamental physics. The public code SModelS [1, 2] provides a very efficient framework for this reinterpretation by decomposing the signal of an arbitrary new physics model (respecting a Z_2 symmetry or a larger symmetry with a Z_2 subgroup) into simplified-model topologies. This then allows us to apply the simplified-model cross-section upper limits or efficiency maps provided by the experimental collaborations (typically as a function of the BSM masses involved) in the context of the new model.¹

So far only BSM searches in final states with missing transverse momentum (MET) could be taken into account within SModelS. However, it has widely been recognized recently that well-motivated BSM theories can provide non-neutral long-lived particles (LLPs) leading to distinct signatures, which often provide great sensitivity at the LHC [7].

A method for (re)using LLP simplified-model constraints was developed previously by some of us in [8]. In this Letter, we now present the implementation of HSCP and R -hadron² signatures in SModelS v1.2 and demonstrate its usability to constrain arbitrary BSM scenarios containing such signatures. The models considered as illustrative examples are the inert doublet model (IDM) and the minimal supersymmetric standard model (MSSM) with a gravitino as the lightest supersymmetric particle (LSP) and a stau next-to-LSP (NLSP). In both cases we concentrate on the cosmologically interesting regions of parameter space which satisfy dark matter constraints.

The IDM provides one of the simplest dark matter models supplementing the standard model by just another SU(2) doublet. While MET searches are scarcely sensitive to the cosmologically allowed region of parameter space, we show that, for small mass splittings within the inert doublet, a large range of dark matter masses can be tested with HSCP searches.

Our second showcase, the gravitino dark matter model, is a cosmologically attractive scenario allowing to alleviate the gravitino problem and to accommodate large reheating temperatures $T_R \sim 10^9$ GeV in the early Universe while respecting

Email addresses: heisig@physik.rwth-aachen.de (Jan Heisig), sabine.kraml@lpsc.in2p3.fr (Sabine Kraml), andre.lessa@ufabc.edu.br (Andre Lessa)

¹A certain degree of approximation results from neglecting properties like the exact production mechanism and the spin of the particles in decays, see Refs. [3–6] for a corresponding discussion.

²For concreteness we label electrically charged but color neutral heavy stable particles as HSCPs. Long-lived colored particles, which can hadronize and form electrically charged bound states are always referred to as R -hadrons.

bounds from big bang nucleosynthesis (BBN) [9]. The complexity of the model reveals a larger number of contributing topologies, including R -hadron signatures relevant for both squarks and gluinos when their decays are 3- or 4-body suppressed. We show that the LLP results have the potential to be competitive with cosmological constraints and impact the allowed range for the reheating temperature.

With respect to previous versions, SMODELS v1.2 includes an additional step in the decomposition accounting for the probabilities of BSM particles to decay promptly or to appear long-lived. Our implementation goes beyond the method presented in [8] by incorporating a better treatment of finite lifetimes (for $c\tau$ of the order of the size of detector) and the inclusion of CMS 13 TeV results. Concretely, we added the experimental cross-section upper limits for the direct production of HSCPs from [10, 11] and R -hadrons from [11], and we developed and included recasted efficiency maps for the 13 TeV analysis [11]. SMODELS v1.2 is publicly available at <http://smodels.hephy.at>.

In the following, Section 2 briefly describes the implementation of LLP signatures into SMODELS. The application to the IDM and gravitino dark matter scenarios is presented in Section 3. Section 4 contains our conclusions. Finally, in Appendix A and Appendix B we provide, respectively, details about the recasting of the HSCP analyses and a discussion about the treatment of intermediate lifetimes.

2. Implementation in SModels

Given the BSM particle masses, quantum numbers, total decay widths, branching ratios (BRs) and total production cross-sections, SMODELS v1.2 performs a decomposition of the input model into a coherent sum of simplified-model topologies. Because of the required Z_2 symmetry, the simplified-model topologies have a two-branch structure from the production of two BSM states followed by their respective cascade decays. We require that each cascade decay terminates with a long-lived particle (which may lead to MET or a visible LLP signature) while all intermediate decays are required to be prompt. By long-lived we mean here and in the following that the particle traverses the whole detector.

At each step in the cascade we compute the probability for the BSM particle to decay promptly ($\mathcal{F}_{\text{prompt}}$) or to decay outside the detector ($\mathcal{F}_{\text{long}}$), which can be relevant for metastable particles with proper lifetimes within few cm to

few m [8]. The respective weight of a topology, $\tilde{\sigma}$, is hence given by:

$$\tilde{\sigma} = \sigma_{\text{prod}} \left(\prod_i \text{BR}_i \times \mathcal{F}_{\text{prompt}}^i \right) \mathcal{F}_{\text{long}}^X \mathcal{F}_{\text{long}}^Y, \quad (1)$$

where σ_{prod} is the production cross-section of the mother particles and X, Y are the BSM final states of the two decay chains; the index i runs over all intermediate BSM particles. Using the particle proper lifetime (τ), $\mathcal{F}_{\text{prompt}}$ and $\mathcal{F}_{\text{long}}$ can be approximated by:

$$\mathcal{F}_{\text{prompt}} = 1 - \exp \left(-\frac{1}{c\tau} \left\langle \frac{\ell_{\text{inner}}}{\gamma\beta} \right\rangle_{\text{eff}} \right) \quad (2)$$

and

$$\mathcal{F}_{\text{long}} = \exp \left(-\frac{1}{c\tau} \left\langle \frac{\ell_{\text{outer}}}{\gamma\beta} \right\rangle_{\text{eff}} \right), \quad (3)$$

where we choose $\langle \ell_{\text{inner}}/\gamma\beta \rangle_{\text{eff}} = 1 \text{ mm}$ and $\langle \ell_{\text{outer}}/\gamma\beta \rangle_{\text{eff}} = 7 \text{ m}$.³ A detailed motivation of the above expressions and values is given in Appendix B. Note that this choice is conservative, since the signature of particles decaying inside the detector may provide additional sensitivity. However, such cases introduce a dependence on the decay products of the long-lived particle which is left for future work.

Topologies terminating in neutral LLPs (including stable neutral BSM particles) lead to the conventional MET signatures, which constitute the bulk of supersymmetry (SUSY) searches already included in the SMODELS database [1, 2, 12]. In order to be able to test also topologies terminating in electrically or color-charged BSM states, we have added the CMS searches for lepton-like HSCPs, color-octet (gluino-like) R -hadrons and color-triplet (squark-like) R -hadrons at 8 TeV [13] and 13 TeV [11] centre-of-mass energies.

For the 8 TeV HSCP results, we make use of the recasting provided in Ref. [10], while a dedicated recasting was performed for the 13 TeV results (see Appendix A for details). This allowed us to compute efficiency maps for the eight simplified-model topologies introduced in Ref. [8], which are included in the SMODELS v1.2 database. For the R -hadron searches we consider only the direct production topology⁴ and make use of the cross-section upper limits from Refs. [11, 13] for the

³This reflects the size of the CMS detector, as we currently have only CMS results included; when including ATLAS results in the future, $\langle \ell_{\text{outer}}/\gamma\beta \rangle_{\text{eff}}$ will have to be adjusted accordingly.

⁴As R -hadrons are strongly produced, their production via cascade decays is typically expected to be less important.

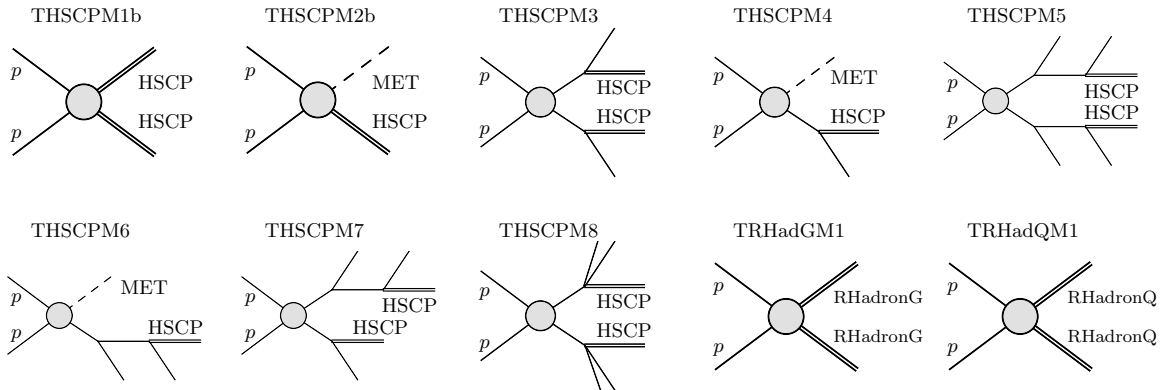


Figure 1: HSCP and R -hadron simplified model topologies included in the SMOBELS v1.2 database. The double lines represent a lepton-like HSCP, a gluino-like or a squark-like R -hadron final state, while dashed lines represent any cascade decay ending up in a neutral LLP (MET signature). The labels of each topology corresponds to the naming convention used in the database. Note that in SMOBELS v1.2 the formalism used for mapping the BSM model topologies to the constraints in the database now includes a list of the BSM final state signatures, e.g. (MET, HSCP).

cloud hadronization model (assuming a 50% probability for \tilde{g} -gluon bound state formation). These limits are also included in the SMOBELS v1.2 database. The relevant topologies and their notation in SMOBELS v1.2 are summarized in Fig. 1.

3. Physics applications

To demonstrate the physics impact, in the following we apply SMOBELS v1.2 to two BSM scenarios and derive the LHC constraints on their parameter space. As mentioned in the introduction, we consider the IDM as well as the MSSM with a gravitino LSP and a stau NLSP as illustrative examples.

3.1. The inert doublet model

The IDM is a two-Higgs doublet model with an exact \mathcal{Z}_2 symmetry, under which all standard model fields (including the Higgs doublet H) are assumed to be even, while the second scalar doublet Φ is odd. It supplements the standard model Lagrangian by the gauge kinetic terms for Φ as well as additional terms in the scalar potential, which now reads

$$\begin{aligned}
 V = & \mu_1^2 |H|^2 + \mu_2^2 |\Phi|^2 + \lambda_1 |H|^4 + \lambda_2 |\Phi|^4 \\
 & + \lambda_3 |H|^2 |\Phi|^2 + \lambda_4 |H^\dagger \Phi|^2 \\
 & + \lambda_5 / 2 [(H^\dagger \Phi)^2 + \text{h.c.}].
 \end{aligned} \tag{4}$$

After electroweak symmetry breaking the model contains five physical scalar states with masses given by

$$\begin{aligned}
 m_{h^0}^2 = & \mu_1^2 + 3\lambda_1 v^2, & m_{H^0}^2 = & \mu_2^2 + \lambda_L v^2, \\
 m_{A^0}^2 = & \mu_2^2 + \lambda_S v^2, & m_{H^\pm}^2 = & \mu_2^2 + \frac{1}{2} \lambda_3 v^2,
 \end{aligned} \tag{5}$$

where

$$\lambda_{L,S} = \frac{1}{2} (\lambda_3 + \lambda_4 \pm \lambda_5). \tag{6}$$

Imposing $m_{h^0} \simeq 125.09$ GeV [14], we are left with five free physical parameters: m_{H^0} , m_{A^0} , m_{H^\pm} , λ_L and λ_2 .

Despite its simplicity, the IDM leads to a rich phenomenology and provides a viable dark matter candidate with observable signatures in direct and indirect detection experiments. For recent accounts see, e.g., [15–17]. At the LHC the IDM is extremely difficult to observe via MET searches [18–23]. For instance, a reinterpretation of dilepton plus MET searches at 8 TeV [24] provides sensitivity up to $m_{H^0} \simeq 55$ GeV only [23]. We checked that current 13 TeV analyses [25, 26] do not significantly change this picture. However, in this low-mass region, the H^0 thermal relic density, Ω_{IDM} , is above the observed dark matter density, Ω_{CDM} . There are in fact three regions where the IDM can account for the entire observed relic density ($55 \text{ GeV} \lesssim m_{H^0} \leq m_{h^0}/2$, $m_{H^0} \simeq 72$ GeV and $m_{H^0} \gtrsim 500$ GeV) and a region where it can account only for a fraction of Ω_{CDM} ($72 \lesssim m_{H^0} \lesssim 500$ GeV) [17, 27].

Considering non-MET signatures the situation is, however, different. As pointed out in [16] the mass-degenerate region $\Delta m \equiv m_{H^\pm} - m_{H^0} \lesssim 1$ GeV is potentially accessible at LHC up to much larger m_{H^0} in searches for long-lived particles. Note also that in the third region mentioned above ($m_{H^0} \gtrsim 500$ GeV) a rather small mass splitting ($|m_{H^0} - m_{A^0/H^\pm}|$ below a few GeV) is required in order to match the relic density constraint [16, 28].

It is therefore interesting to focus on this region with small mass splittings, $\Delta m \lesssim 1$ GeV, and use SMOBELS v1.2 to reinterpret the LHC limits from HSCP searches within the IDM model. For this

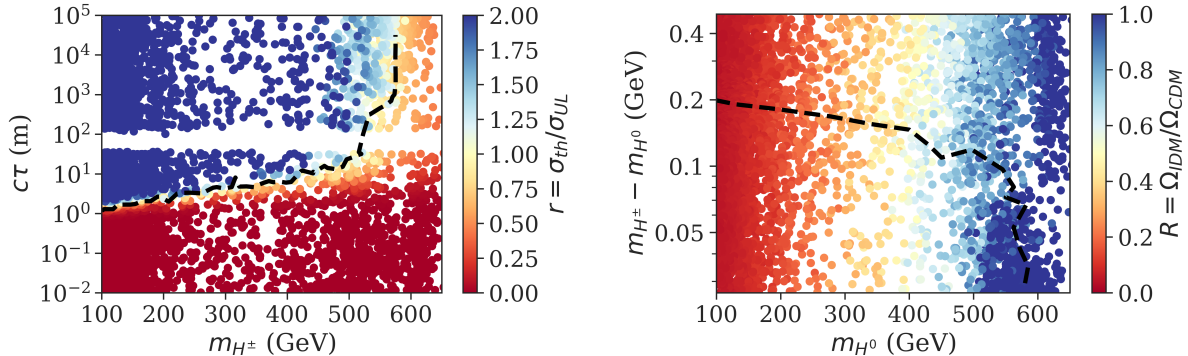


Figure 2: Allowed IDM parameter points (imposing all but the LHC constraints) in the m_{H^\pm} vs. $c\tau$ plane (left panel) and m_{H^\pm} vs. Δm (right panel). The colour denotes the LHC signal strength r and the dark matter fraction R , respectively. The black dashed curves show the (interpolated) 95% CL exclusion contour from the LHC ($r = 1$).

purpose we perform a scan over the 5-dimensional parameter space:

$$\begin{aligned}
100 \text{ GeV} &\leq m_{H^0} \leq 1 \text{ TeV} \\
m_{H^0} &< m_{A^0} \leq 1.1 \text{ TeV} \\
10 \text{ MeV} &\leq m_{H^\pm} - m_{H^0} \leq 1 \text{ GeV} \\
-4\pi &\leq \lambda_L \leq 4\pi \\
10^{-6} &\leq \lambda_2 \leq 4\pi
\end{aligned} \tag{7}$$

imposing $10^{-3} \leq R \equiv \Omega_{\text{IDM}}/\Omega_{\text{CDM}} \leq 1$; Ω_{IDM} is computed with MICROMEAS [29, 30] and we assume a 10% uncertainty on the prediction. In addition, following Ref. [17], we take into account constraints from Higgs invisible decays [31], electroweak precision observables [32, 33], from searches for charginos and neutralinos at LEP-II [18, 34], indirect detection limits from γ -ray observations of dwarf spheroidal galaxies [35] and theoretical constraints on unitarity, perturbativity and vacuum stability computed with 2HDMC [33].⁵ We use the nested-sampling algorithm MULTINEST [37, 38] to efficiently explore the parameter space. In the following we only consider points allowed within the 2σ region of the global fit [17].

For the allowed parameter space we compute the decay tables and production cross-sections with MADGRAPH5_AMC@NLO [39] and evaluate the LHC constraints with SMOBELS v1.2. For each parameter space point, the constraining power of LHC searches can be conveniently parametrized by the ratio of the relevant signal cross-section, σ_{th} , to the corresponding analysis upper limit, σ_{UL} : $r \equiv \sigma_{\text{th}}/\sigma_{\text{UL}}$ (see Ref. [2] for details). If $r \geq 1$ for at least one analysis, we consider the point as excluded.

⁵With respect to Ref. [17], in this work we update direct detection constraints, additionally imposing the 90% CL upper limits on the spin-independent dark matter-nucleon scattering cross-section recently obtained by Xenon1T [36].

The results are shown in Fig. 2. In the left panel we display the signal strength r in the m_{H^\pm} vs. $c\tau$ plane, while the right panel shows the dark matter fraction R in the m_{H^0} vs. Δm plane. Although r does depend on all the model parameters, it is mostly driven by the mass and lifetime of charged Higgs. We hence show an approximate exclusion curve in the plot (dark dashed curve). In all the parameter space considered, we have verified that the exclusion is completely dominated by the HSCP searches; even though the MET constraints were also applied, they could not exclude any of the points.

In the quasi-stable limit ($c\tau \gtrsim 10^3$ m) HSCP searches exclude H^\pm masses up to 580 GeV. This limit goes beyond the 13 TeV LHC limit for direct production of detector-stable staus which reaches $m_{\tilde{\tau}} = 360$ GeV [11]. The reason for the higher reach is the appearance of the additional W -mediated production channel $pp \rightarrow H^0 H^\pm$ as well as (to a lesser extent and depending on m_{A^0}) the channels $pp \rightarrow A^0 H^\pm, A^0 A^0$ with $A^0 \rightarrow H^\pm$. As an example, for $m_{H^0} \simeq m_{A^0} \simeq m_{H^\pm} \simeq 520$ GeV we have $\sigma(H^\pm H^\pm) + \sigma(H^\pm H^0) + \sigma(H^\pm A^0) \simeq 1.14$ fb against $\sigma(\tilde{\tau}\tilde{\tau}) \simeq 0.15$ fb [11] for the same stau mass.

At the lower edge of our scan range, for $m_{H^\pm} \simeq m_{H^0} \gtrsim 100$ GeV, HSCP searches are able to constrain decay lengths down to around $c\tau \simeq 2$ m. Here the significant exponential suppression of $\mathcal{F}_{\text{long}}$ is compensated by the large cross-section. Note that our choice for $\langle \ell_{\text{outer}}/\gamma\beta \rangle_{\text{eff}}$ leads to a somewhat conservative exclusion limit in this part of the parameter space (see Appendix B, left panel of Fig. B.6).

Let us also point out that the calculation of $c\tau$ involves a certain degree of approximation. In particular, the decays are computed at leading order with MADGRAPH5_AMC@NLO, where the decay channels with first generation quarks in the

final state are turned off for Δm below the pion mass. This introduces the (artificial) gap seen at $c\tau \sim 100$ m, which would not appear if the proper phase-space including the pion mass were considered.

In the right panel of Fig. 2, we show the HSCP exclusion curve in the Δm vs. m_{H^0} plane. It excludes a significant part of the parameter space with $\Delta m \lesssim 0.2$ GeV. Interestingly, the HSCP searches are starting to exclude part of the region with $R = 1$, where the IDM can account for the entire observed relic density ($m_{H^0} \gtrsim 500$ GeV). Note that disappearing track searches have the potential to further extend the reach towards larger Δm [16].

3.2. Gravitino dark matter scenario

The gravitino – the superpartner of the graviton – is an attractive dark matter candidate in supersymmetric theories. A gravitino (\tilde{G}) LSP is also interesting from the model-building point of view. Due to strong BBN constraints for gravitinos that decay into lighter sparticles, an unstable gravitino is either required to be extremely heavy or the reheating temperature has to be kept small [40]. While the former limits the viable options for supersymmetry breaking, the latter reduces the options for possible baryogenesis mechanisms. In the gravitino DM scenario these problems can be circumvented. Thermal gravitino production however still imposes strong constraints on the maximal reheating temperature to avoid overclosure of the universe [41].

Once the gravitino is the LSP, the lightest sparticle of the MSSM (i.e. the NLSP) can be any sparticle. However, in order to not reintroduce severe constraints from BBN due to late decays of the NLSP [42], certain choices appear more promising than others. For instance, the stau is an attractive NLSP candidate providing a large annihilation cross-section, thus resulting in smaller freeze-out abundances. Moreover, $\tilde{\tau} \rightarrow \tau\tilde{G}$ decays inject less hadronic (and electromagnetic) energy than the decays of various other NLSP candidates, e.g., $\tilde{\chi}_1^0 \rightarrow Z/\gamma + \tilde{G}$. As a consequence, the impact of the late time stau decays on BBN is reduced. At the same time, it also reduces the contribution to the gravitino abundance through NLSP decays. This allows for a larger thermal contribution of gravitino production while not over-closing the Universe. Since the thermal contribution is (approximately) proportional to the reheating temperature, $\Omega_{\tilde{G}}^{\text{th}} \propto T_{\text{R}}$ [41, 43, 44], it allows for higher values of T_{R} , as preferred by classes of models for leptogenesis and inflation.⁶

⁶We note that these arguments simply serve to motivate

We here consider the gravitino DM scenario with a stau NLSP, revisiting the parameter scan performed in [9, 45] refining and updating the constraints from LLP searches at the LHC. The scan was performed within the framework of the so-called phenomenological MSSM (pMSSM) with the additional assumption $m_{\tilde{q}_{1,2}} \equiv m_{\tilde{Q}_{1,2}} = m_{\tilde{u}_{1,2}} = m_{\tilde{d}_{1,2}}$. In this way a 17-dimensional parameter space was achieved with input parameters and scan ranges given by:⁷

$$\begin{aligned}
-10 \text{ TeV} &\leq A_t &&\leq 10 \text{ TeV} \\
-8 \text{ TeV} &\leq A_b, A_\tau, \mu &&\leq 8 \text{ TeV} \\
1 &\leq \tan \beta &&\leq 60 \\
100 \text{ GeV} &\leq m_A &&\leq 4 \text{ TeV} \\
200 \text{ GeV} &\leq m_{\tilde{\tau}_1} &&\leq 2 \text{ TeV} \\
700 \text{ GeV} &\leq m_{\tilde{t}_1}, m_{\tilde{b}_1} &&\leq 5 \text{ TeV} \\
0 &< \theta_{\tilde{\tau}}, \theta_{\tilde{t}} &&< \pi \\
m_{\tilde{\tau}_1} &\leq m_{\tilde{L}_{1,2}}, m_{\tilde{e}_{1,2}} &&\leq 4 \text{ TeV} \\
1.2 \text{ TeV} &\leq m_{\tilde{q}_{1,2}} &&\leq 8 \text{ TeV} \\
m_{\tilde{\tau}_1} &\leq M_1, M_2 &&\leq 4 \text{ TeV} \\
1 \text{ TeV} &\leq M_3 &&\leq 5 \text{ TeV}
\end{aligned} \tag{8}$$

The particle spectrum was computed with SUSPECT 2.41 [46] and FEYNHIGGS 2.9.2 [47]. All points were required to have the lighter stau $\tilde{\tau}_1$ as the NLSP. Moreover, $m_h \in [123; 128]$ GeV [14, 48] was imposed.

The decay widths and branching ratios were computed with SDECAY [49, 50] and (in the case of missing dominant decay channels) MADGRAPH5_AMC@NLO [39], while the freeze-out abundance of staus was computed with MICROMEGAS [29]. The analysis considered constraints on the MSSM Higgs sector from LEP, the Tevatron and the LHC, EW precision bounds as well as theoretical constraints arising from charge or color breaking vacua; see [45] for details and references. In addition, we here impose updated flavor constraints: $\text{BR}(B \rightarrow X_s \gamma) \in [3.0; 3.64] \times 10^{-4}$ [51] and $\text{BR}(B_s^0 \rightarrow \mu^+ \mu^-) \in [1.74; 4.34] \times 10^{-9}$ [52]. Moreover, updated limits on the MSSM Higgs sector are included by applying the conservative constraints on m_A and $\tan \beta$ derived in the $m_h^{\text{mod}+}$ scenario [53].

our choice of a stau NLSP, but do not exclude other NLSP candidates.

⁷In this phenomenologically driven parameter scan the spectrum parameters of the third generation sfermions, $m_{\tilde{\tau}_1}$, $m_{\tilde{t}_1}$, $m_{\tilde{b}_1}$, $\theta_{\tilde{\tau}}$ and $\theta_{\tilde{t}}$, were chosen as input parameters in order to obtain an equally good coverage of small and large mixing scenarios. Tree-level relations were used to translate these parameters into soft parameters. In the further analysis only the values recalculated by the spectrum generator are used consistently.

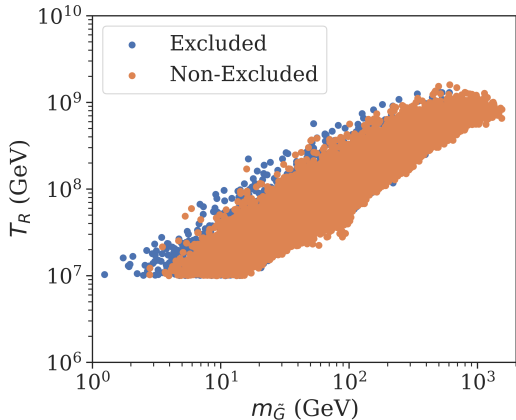


Figure 3: Effect of the LHC exclusion bounds on the otherwise allowed points in the plane spanned by the gravitino mass and reheating temperature.

Since the gravitino mass can be taken as an additional free parameter, for each point in the pMSSM parameter space satisfying the above requirements, 10 gravitino masses are randomly generated. They are required to lie within an interval where the total \tilde{G} abundance can match the measured dark matter abundance:

$$\Omega_{\tilde{G}}^{\text{non-th}} h^2 + \Omega_{\tilde{G}}^{\text{th}} h^2 = \Omega_{\text{CDM}} h^2, \quad (9)$$

where $\Omega_{\tilde{G}}^{\text{th}} h^2$ and $\Omega_{\tilde{G}}^{\text{non-th}} h^2$ are the thermal and non-thermal gravitino relic abundances, respectively. The latter is generated once the frozen-out $\tilde{\tau}$ s decay to \tilde{G} s, thus enhancing the total gravitino abundance. The former is determined mostly by the gravitino mass, the gaugino masses and the reheating temperature, T_R [41, 43, 44]. Given a pMSSM point and gravitino mass, first $\Omega_{\tilde{G}}^{\text{non-th}} h^2$ is computed and from this the reheating temperature imposing eq. (9) with $\Omega_{\text{CDM}} h^2 = 0.1189$, taking into account the contributions from the complete spectrum. For each of the resulting points in the (17+1)-dimensional parameter space (that by construction fulfills the relic density constraint), constraints from BBN [54, 55] are imposed (see Ref. [9] for further details).

After selecting around 26k points satisfying the above constraints, we use SMOBELS v1.2 to decompose each point's LHC signal into all relevant simplified-model topologies, taking into account the production and cascade decays of all sparticles. The LO production cross-sections are computed with PYTHIA 8 [56, 57]; NLL cross-sections for $\tilde{g}\tilde{g}$, $\tilde{g}\tilde{q}$ and $\tilde{q}\tilde{q}$ are then obtained using NLLFAST [58–64]. The results from the 8 TeV and 13 TeV HSCP and R -hadron searches implemented in SMOBELS v1.2 are then applied in order to constrain the points. Note that, since all the cascade decays terminate (at collider scales) in

the stau NLSP or in R -hadrons, MET constraints do not apply.

From all the tested points, $\sim 5\text{k}$ are excluded and $\sim 21\text{k}$ are allowed, as shown in Fig. 3. For a fixed gravitino mass (below ~ 200 GeV), the largest values of T_R are excluded by the LHC constraints. This is due to the fact that the largest reheating temperatures are typically achieved for points with small gluino masses, which in turn contain large production cross-sections at the LHC. As a result these points can be probed by the HSCP and R -hadron searches. We see, however, that the largest values of T_R ($\simeq 10^9$ GeV) obtained in the scan are still allowed by the LHC constraints obtained with SMOBELS.

In order to discuss which searches and topologies are relevant for testing the gravitino scenario, we show in Fig. 4 a histogram for the number of excluded points as a function of the gluino mass. In the left panel, the number of excluded points is grouped according to which is the most constraining type of signature. The stacked histogram shows that the bulk of the points are excluded by topologies containing HSCP signatures, as expected. Nonetheless, a significant fraction of points at low $m_{\tilde{g}}$ are excluded by R -hadron constraints for long-lived gluinos. These points typically have heavy squarks, resulting in suppressed 3-body or 4-body gluino decays. In a similar way, points with light squarks and heavy gauginos and higgsinos lead to long-lived squarks which can also be constrained by the R -hadron searches, as shown by the orange histogram.

In order to illustrate the constraining power of combining results for multiple simplified-model topologies, we also display (dark blue histogram) the distribution of excluded points obtained using only the CMS limits for pair production of long-lived staus, gluinos and squarks. As can be seen, the number of excluded points in this case (~ 200) is drastically reduced when compared to the one obtained with all the topologies included in SMOBELS. We point out, however, that the constraining power of SMOBELS is still limited by the number of simplified-model results contained in its database. The points from the pMSSM scan performed here display a large variety of topologies and many of them do not fall within the eight HSCP or the two R -hadron topologies included in the database.

SMOBELS can also conveniently be used to identify the most relevant missing topologies. In the right panel of Fig. 4, we show the non-excluded points with a total SUSY production cross-section (at 13 TeV) larger than 5 fb. Due to their sizeable cross-section, such points have a potential for being excluded by the HSCP or R -hadron searches.

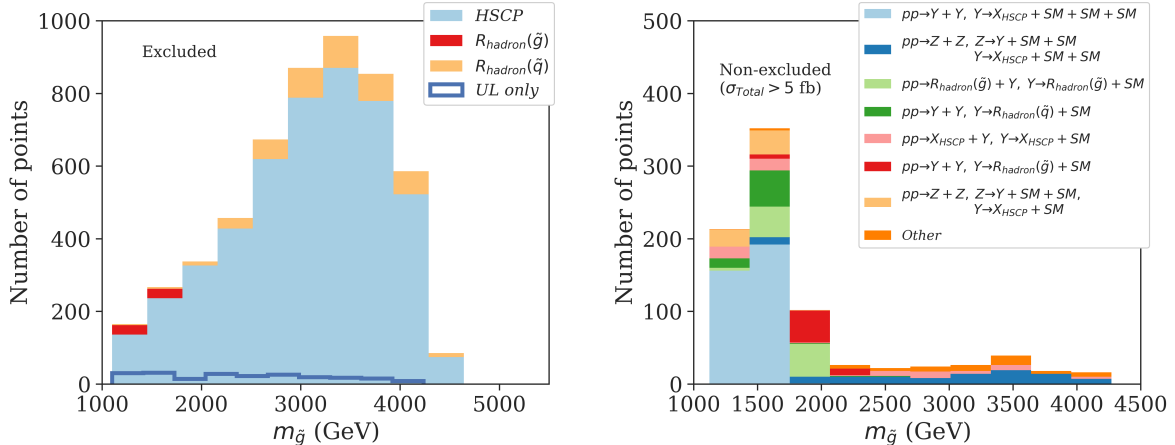


Figure 4: Left panel: Number of excluded points as a function of the gluino mass. The colour indicates the most constraining type of signature. The solid blue histogram displays the number of points excluded when imposing only the CMS limits on the direct pair production of HSCPs and R -hadrons. Right panel: Number of non-excluded points with a total SUSY production cross-section of more than 5 fb at 13 TeV. The colour indicates the simplified-model topology with largest weight (cross-section times branching ratio).

The stacked histogram shows the distribution of non-excluded points as a function of the gluino mass grouped according to the missing topology with largest weight (cross-section times branching ratio). Most of the points have $m_{\tilde{g}} < 1.7$ TeV, since this ensures $\sigma(\tilde{g}\tilde{g}) \gtrsim 5$ fb. The almost flat distribution at large $m_{\tilde{g}}$ corresponds to points with light squarks in the spectrum, thus also resulting in large total cross-sections.

We see that the missing topology which occurs more often in Fig. 4 (light blue histogram) corresponds to pair production of BSM particles, which then go through 4-body decays to the HSCP. This topology is mostly generated by points with very light gluinos, which then decay directly to the $\tilde{\tau}$ through 4-body decays. Furthermore, we see that topologies with 1-step decays to R -hadrons (green and dark red histograms) might also give potentially powerful constraints on this scenario. These topologies often appear in points with light quarks (gluinos) which decay to long-lived gluinos (quarks).

4. Conclusions

Long-lived particles have received increasing attention from both the experimental and theoretical communities, due to their novel collider signatures and possible connection to dark matter.

In this Letter we discussed how some of the LHC searches for LLPs, interpreted in the context of simplified models, can provide a powerful means for constraining interesting dark matter scenarios. For this purpose, we presented an implementation of (lepton-like) HSCP and (gluino-

and squark-like) R -hadron signatures into SMOODELS. The SMOODELS database was extended by official CMS simplified-model results from the 8 and 13 TeV runs of the LHC, as well as additional efficiency maps obtained from a recast of the CMS analyses.

We then used the new version of SMOODELS, v1.2, to investigate how these searches impact two concrete physics scenarios: the Inert Doublet Model and a gravitino dark matter model containing long-lived staus. While missing-energy searches are not able to constrain any significant part of the cosmologically interesting parameter space of the IDM, we found that, for small mass splittings within the inert doublet of $\Delta m \lesssim 0.2$ GeV, HSCP searches are sensitive to dark matter masses of up to 580 GeV. The gravitino dark matter model, on the other hand, can be constrained by both HSCP and R -hadron searches, and we showed how SMOODELS can be used to derive constraints on the reheating temperature which are complementary to cosmological bounds.

The current version of SMOODELS is easily extendible to include additional new simplified-model results from searches for detector-stable LLPs from both CMS and ATLAS. The inclusion of other types of LLP signatures, for example displaced vertices, is more involved and left for future developments of the code.

Acknowledgements

We thank Nishita Desai, Suchita Kulkarni, Ursula Laa and Wolfgang Waltenberger for helpful discussions. Moreover, very special thanks go to

Wolfgang Waltenberger for helping with the public release of the code.

This work is supported by the German Research Foundation DFG through the research unit “New physics at the LHC”. S.K. is supported by the IN2P3 project “Théorie – LHC-iTools” and the CNRS-FAPESP collaboration grant PRC275431. A.L. is supported by the Sao Paulo Research Foundation (FAPESP), projects 2015/20570-1 and 2016/50338-6.

Appendix A. Recasting and validation

In this appendix we detail the recasting of the 8 and 13 TeV HSCP searches used in SMODELS v1.2. We first review the recasting for the 8 TeV CMS HSCP analysis presented in [10]. The authors of [10] provide signature efficiencies for the off- and online selection criteria, $P_{\text{on}}(\mathbf{k})$ and $P_{\text{off}}(\mathbf{k})$, respectively, as a function of the generator-level kinematics, $\mathbf{k} = (\eta, p_T, \beta)$, of isolated⁸ HSCP candidates. The signal efficiency for a given parameter point can be computed from the generated events:

$$(\mathcal{A}\epsilon) = \frac{1}{N} \sum_{i=1}^N \mathcal{P}_{\text{event}}^i \quad (\text{A.1})$$

where the sum runs over all N events and

$$\mathcal{P}_{\text{event}}^i = \mathcal{P}_{\text{on}}^i \times \mathcal{P}_{\text{off}}^i \quad (\text{A.2})$$

with

$$\begin{aligned} \mathcal{P}_{\text{on/off}}^i &= P_{\text{on/off}}(\mathbf{k}_1^i) + P_{\text{on/off}}(\mathbf{k}_2^i) \\ &\quad - P_{\text{on/off}}(\mathbf{k}_1^i) \times P_{\text{on/off}}(\mathbf{k}_2^i). \end{aligned} \quad (\text{A.3})$$

For one HSCP candidate in an event the formula holds with $P_{\text{on/off}}(\mathbf{k}_2^i) = 0$.

Using the efficiencies computed from (A.1) for the direct pair production of staus and the observed and expected number of background events (along with its error) from Ref. [10], we obtain upper limits for the stau cross-section as a function of the stau mass. These can then be directly compared to the CMS values presented in Ref. [10]. The left panel of Fig. A.5 shows the CMS and our results for the cross-section upper limits (upper frame) as well as their ratio (lower frame). As we can see, the difference is always below 5% and compatible with Monte Carlo errors. Hence we expect that recasting uncertainties for the efficiencies computed with the above method and included in the SMODELS database should only be of a few percent.

⁸Details on the imposed isolation criteria can be found in [8, 10].

For the respective 13 TeV analysis [11], however, such a recast has not yet been provided by the collaboration. Nonetheless, since the trigger and selection criteria of the 8 and 13 TeV analyses are very similar, we expect that the signal efficiencies from the 13 TeV search do not differ drastically from the 8 TeV ones. The two analyses only differ in a slightly stronger cut on the ionization loss and time-of-flight, which effectively amounts to a slightly stronger cut on the HSCP velocity in the latter analysis.⁹

Ref. [65] reported an attempt to model the 13 TeV signature efficiencies by multiplying the 8 TeV ones with a velocity dependent correction function fitted in order to resemble the signal efficiencies reported in [11]. On top of the slight reduction of the signature efficiencies for high velocities, this study revealed a better performance of the CMS detector in the region of low velocities leading to larger signal efficiencies for large HSCP masses. This latter feature could, however, not be described by a universal velocity dependent correction function for direct pair production and inclusive production. In order for a proper understanding of the differences between Runs 1 and 2, further information (which is not publicly available) is needed.

Therefore we choose to follow a conservative approach taking into account the reduction in the efficiency due to the slightly stronger cuts on the velocity of the HSCP candidate. We model this by multiplying $P_{\text{off}}(\mathbf{k})$ with a correction function which is assumed to depend only on β :

$$f_{(a,b)}^{\text{corr}}(\beta) = \left(1 + e^{a(\beta-b)}\right)^{-1} \leq 1. \quad (\text{A.4})$$

We determine the parameters a, b in a global fit to the signal efficiencies for the pair production and inclusive production model reported in Ref. [11]. To this end we define the χ^2 function:

$$\chi^2 = \sum_m \frac{\left((\mathcal{A}\epsilon)_{(a,b)}^m - (\mathcal{A}\epsilon)_{\text{CMS}}^m\right)^2}{\sigma_{\mathcal{A}\epsilon}^2}, \quad (\text{A.5})$$

where $(\mathcal{A}\epsilon)_{(a,b)}^m$ is the signal efficiency for a mass point m of the considered model using the signature efficiencies with the correction function $f_{(a,b)}^{\text{corr}}$ and $(\mathcal{A}\epsilon)_{\text{CMS}}^m$ is the respective signal efficiency reported by CMS in Ref. [11]. The characteristic size of the uncertainty, $\sigma_{\mathcal{A}\epsilon}$, is (arbitrarily) set to 0.02, which roughly reflects the precision of the recasting we aim at.

⁹The effect of a slightly stronger cut on p_T [11] is found to be negligible for masses of a few hundred GeV.

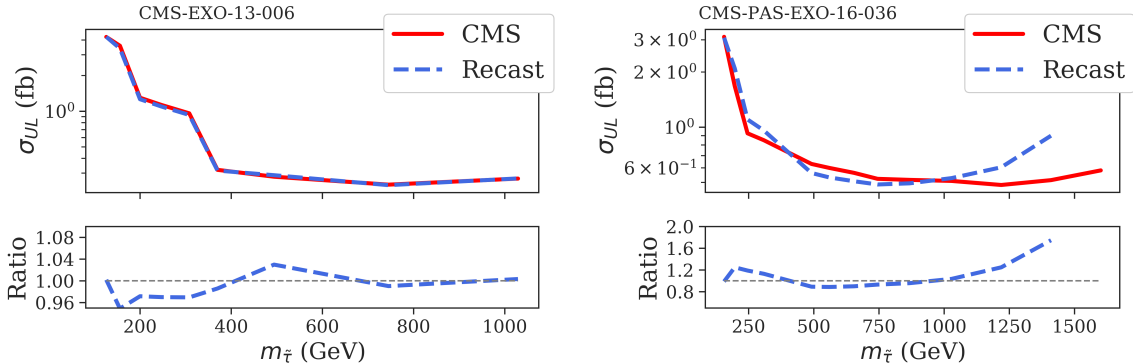


Figure A.5: Validation of the 8 TeV (left) and 13 TeV (right) CMS analysis for direct production of staus. The red and blue dashed curves in the upper panels show, respectively, the cross-section upper limits from CMS and from our recast. The lower frames show the ratio between our recast and the CMS results.

We minimize the χ^2 using MULTINEST [37, 38] and obtain the best-fit parameters $a \simeq 500$ and $b = 0.807$. This fit uses all the 12 benchmark points (6 for direct stau production and 6 for inclusive production) considered in Ref. [11] and for which signal efficiencies were reported. We verified that very similar results are obtained when using only a subset of the benchmark points.

Once again we compare the upper limits for the total stau direct production cross-section obtained using our recast procedure and the ones reported by CMS. The comparison is shown in the right panel of Fig. A.5, where we see that, despite having a worse agreement than the 8 TeV results, the 13 TeV upper limits are within 20% while for large range of stau masses. Only for $m_{\tilde{\tau}} \gtrsim 1.2$ TeV the recasting significantly diverges from the official values. We point out, however, that the results are still conservative due to the above mentioned effects.

Appendix B. Finite lifetimes

Although the LLP searches considered here are aimed at detector-stable particles, they can also constrain models with intermediate decay length of the order of the detector size, where only a certain fraction of particles decay after traversing the entire sensitive detector. In this case the fraction of long-lived particles, $\mathcal{F}_{\text{long}}$, may be significantly smaller than one and the resulting signal efficiency becomes sensitive to the value chosen for $L_{\text{eff}} \equiv \langle \ell_{\text{outer}} / \gamma \beta \rangle_{\text{eff}}$ (see eq. (3)). Here we discuss in detail what are the expected values for L_{eff} and justify our choice, $L_{\text{eff}} = 7$ m, implemented in SMODELS v1.2 and used in the results presented in Section 3.

The precise value of $\mathcal{F}_{\text{long}}$ (and hence L_{eff}) depends on the input model and experimental analysis and requires a full Monte Carlo simulation for each model point in order to determine the boost

distribution of the LLPs. However, since SMODELS aims for a fast (although approximate) computation of LHC constraints for a large variety of BSM models, our goal is to determine an average value for L_{eff} which can approximately reproduce the correct value of $\mathcal{F}_{\text{long}}$ obtained from a full simulation. Before we can justify this approximation, we must first discuss how to obtain $\mathcal{F}_{\text{long}}$ from the full simulation for a given input model.

We first define the probability F_{long} for a (metastable) particle with momentum \mathbf{k} to decay outside the detector in a given event:

$$F_{\text{long}}(\mathbf{k}) = \exp\left(-\frac{\ell_{\text{outer}}(|\eta|) \frac{1}{\gamma\beta}}{c\tau}\right). \quad (\text{B.1})$$

Here $\gamma = (1 - \beta^2)^{-1/2}$ and $\ell_{\text{outer}}(|\eta|)$ is the travel length through the CMS detector, which we approximate by considering a cylindrical volume with radius of 7.4 m and length of 10.8 m. Using now the off- and online efficiencies (P_{on} and P_{off}) discussed in Appendix A, we can extend the signal efficiency calculation from eq. (A.1) to the case of finite lifetimes using:

$$\begin{aligned} \mathcal{P}_{\text{event}}^i &= F_{\text{long}}(\mathbf{k}_1^i) P_{\text{on}}(\mathbf{k}_1^i) P_{\text{off}}(\mathbf{k}_1^i) (1 - F_{\text{long}}(\mathbf{k}_2^i)) \\ &\quad + F_{\text{long}}(\mathbf{k}_2^i) P_{\text{on}}(\mathbf{k}_2^i) P_{\text{off}}(\mathbf{k}_2^i) (1 - F_{\text{long}}(\mathbf{k}_1^i)) \\ &\quad + F_{\text{long}}(\mathbf{k}_1^i) F_{\text{long}}(\mathbf{k}_2^i) \mathcal{P}_{\text{on}}^i \mathcal{P}_{\text{off}}^i, \end{aligned} \quad (\text{B.2})$$

where $F_{\text{long}}(\mathbf{k}_j^i)$ is the decay probability from eq. (B.1) for the j -th particle in the i -th event.

Using eqs. (B.2) and (A.1) we can then compute the total signal efficiency for a given input model taking into account the correct finite lifetime suppression factor. This efficiency can then be compared to the one computed with SMODELS using $\mathcal{F}_{\text{long}}$ to extract the precise value for L_{eff} given a specific input model.

In Fig. B.6 we consider the direct production of staus (left panel) and direct production of squarks

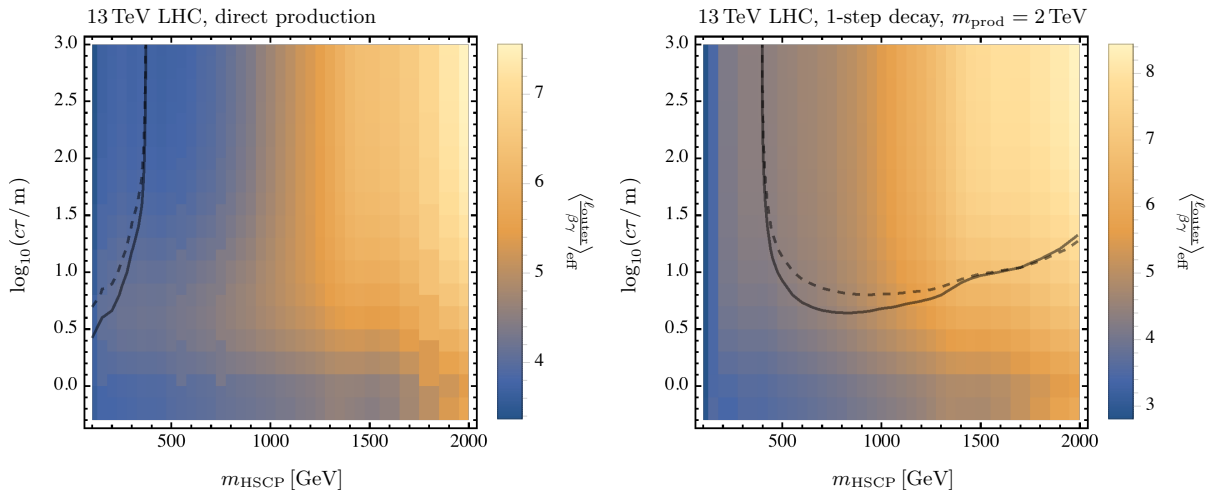


Figure B.6: The effective characteristic travel length, $\langle \ell_{\text{outer}}/\gamma\beta \rangle_{\text{eff}}$ in the parameter plane spanned by the HSCP mass, m_{HSCP} , and its proper decay length, $c\tau$, for direct production (left panel) and for the 1-step decay topology where we choose $m_{\text{prod}} = 2 \text{ TeV}$ for the mass of the produced mother particle (right panel). The solid and dashed curves denote the 95% CL exclusion for the event-based computation of $\ell/\gamma\beta$ and for the approximation choosing $\langle \ell_{\text{outer}}/\gamma\beta \rangle_{\text{eff}} = 7 \text{ m}$, respectively. For the direct production we choose the cross-section Drell-Yan stau pair production, while the cross-section for 1-step decay corresponds to (degenerate) squark production with $m_{\tilde{q}} = m_{\tilde{g}}$.

followed by a 1-step decay into the HSCP at the 13 TeV LHC. In both cases we vary the HSCP mass and lifetime, with $m_{\tilde{g}} = m_{\tilde{q}} = 2 \text{ TeV}$ in the second case. The colour of each point in the plane shows the correct value for $L_{\text{eff}} = \langle \ell_{\text{outer}}/\gamma\beta \rangle_{\text{eff}}$ which should be used in SModelS in order for the signal efficiencies to exactly match the full simulation values.

As we can see, L_{eff} does not vary significantly, spanning values of about 4–8 m. Therefore, in order to remain conservative and at the same time avoid (significantly) underestimating the signal efficiency, we choose $L_{\text{eff}} = 7 \text{ m}$ (or $\ell_{\text{outer}} \simeq 10 \text{ m}$ and $\gamma\beta \simeq 1.43$). Figure B.6 compares the exclusion curves obtained with SModelS v1.2 using this approximation (dashed lines) to the ones obtained using the full simulation (solid lines). Although the SModelS curves are conservative, we see that they agree quite well with the full simulation in most of the parameter space. We have checked that this also holds for other masses and topologies, though for the sake of conciseness do not show these results. We therefore conclude that using a fixed $L_{\text{eff}} = 7 \text{ m}$ value is a valid approximation.

References

- [1] S. Kraml, S. Kulkarni, U. Laa, A. Lessa, W. Magerl, D. Proschofsky-Spindler, and W. Waltenberger, *SModelS: a tool for interpreting simplified-model results from the LHC and its application to supersymmetry*. Eur. Phys. J. **C74** (2014) 2868, [arXiv:1312.4175 \[hep-ph\]](#).
- [2] F. Ambrogio, S. Kraml, S. Kulkarni, U. Laa, A. Lessa, V. Magerl, J. Sonneveld, M. Traub, and W. Waltenberger, *SModelS v1.1 user manual: Improving simplified model constraints with efficiency maps*. Comput. Phys. Commun. **227** (2018) 72–98, [arXiv:1701.06586 \[hep-ph\]](#).
- [3] L. Edelhäuser, J. Heisig, M. Krämer, L. Oymanns, and J. Sonneveld, *Constraining supersymmetry at the LHC with simplified models for squark production*. JHEP **12** (2014) 022, [arXiv:1410.0965 \[hep-ph\]](#).
- [4] L. Edelhäuser, M. Krämer, and J. Sonneveld, *Simplified models for same-spin new physics scenarios*. JHEP **04** (2015) 146, [arXiv:1501.03942 \[hep-ph\]](#).
- [5] C. Arina, M. E. C. Catalan, S. Kraml, S. Kulkarni, and U. Laa, *Constraints on sneutrino dark matter from LHC Run 1*. JHEP **05** (2015) 142, [arXiv:1503.02960 \[hep-ph\]](#).
- [6] S. Kraml, U. Laa, L. Panizzi, and H. Prager, *Scalar versus fermionic top partner interpretations of $t\bar{t} + E_T^{\text{miss}}$ searches at the LHC*. JHEP **11** (2016) 107, [arXiv:1607.02050 \[hep-ph\]](#).
- [7] *Searches for long-lived particles beyond the Standard Model at the Large Hadron Collider*. White paper of the LHC LLP Community, CERN, 2018, *in preparation*.
- [8] J. Heisig, A. Lessa, and L. Quertenmont, *Simplified Models for Exotic BSM Searches*. JHEP **12** (2015) 087, [arXiv:1509.00473 \[hep-ph\]](#).
- [9] J. Heisig, *Gravitino LSP and leptogenesis after the first LHC results*. JCAP **1404** (2014) 023, [arXiv:1310.6352 \[hep-ph\]](#).
- [10] CMS Collaboration, V. Khachatryan *et al.*, *Constraints on the pMSSM, AMSB model and on other models from the search for long-lived charged particles in proton-proton collisions at $\sqrt{s} = 8 \text{ TeV}$* . Eur. Phys. J. **C75** (2015) no. 7, 325, [arXiv:1502.02522 \[hep-ex\]](#).
- [11] CMS Collaboration, V. Khachatryan *et al.*, *Search for heavy stable charged particles with 12.9 fb^{-1} of 2016 data*, Tech. Rep. CMS-PAS-EXO-16-036, 2016. <http://cds.cern.ch/record/2205281>.

- [12] J. Dutta, S. Kraml, A. Lessa, and W. Waltenberger, *SModelS extension with the CMS supersymmetry search results from Run 2*. LHEP **1** (2018) no. 1, 5–12, [arXiv:1803.02204 \[hep-ph\]](#).
- [13] CMS Collaboration, S. Chatrchyan *et al.*, *Searches for long-lived charged particles in pp collisions at $\sqrt{s}=7$ and 8 TeV*. JHEP **07** (2013) 122, [arXiv:1305.0491 \[hep-ex\]](#).
- [14] Particle Data Group Collaboration, K. A. Olive *et al.*, *Review of Particle Physics*. Chin. Phys. **C38** (2014) 090001.
- [15] A. Ilnicka, M. Krawczyk, and T. Robens, *Inert Doublet Model in light of LHC Run I and astrophysical data*. Phys. Rev. **D93** (2016) no. 5, 055026, [arXiv:1508.01671 \[hep-ph\]](#).
- [16] A. Belyaev, G. Cacciapaglia, I. P. Ivanov, F. Rojas-Abatte, and M. Thomas, *Anatomy of the Inert Two Higgs Doublet Model in the light of the LHC and non-LHC Dark Matter Searches*. Phys. Rev. **D97** (2018) no. 3, 035011, [arXiv:1612.00511 \[hep-ph\]](#).
- [17] B. Eiteneuer, A. Goudelis, and J. Heisig, *The inert doublet model in the light of Fermi-LAT gamma-ray data: a global fit analysis*. Eur. Phys. J. **C77** (2017) no. 9, 624, [arXiv:1705.01458 \[hep-ph\]](#).
- [18] A. Pierce and J. Thaler, *Natural Dark Matter from an Unnatural Higgs Boson and New Colored Particles at the TeV Scale*. JHEP **0708** (2007) 026, [arXiv:hep-ph/0703056 \[HEP-PH\]](#).
- [19] Q.-H. Cao, E. Ma, and G. Rajasekaran, *Observing the Dark Scalar Doublet and its Impact on the Standard-Model Higgs Boson at Colliders*. Phys. Rev. D **76** (2007) 095011, [arXiv:0708.2939 \[hep-ph\]](#).
- [20] E. Dolle, X. Miao, S. Su, and B. Thomas, *Dilepton Signals in the Inert Doublet Model*. Phys. Rev. D **81** (2010) 035003, [arXiv:0909.3094 \[hep-ph\]](#).
- [21] X. Miao, S. Su, and B. Thomas, *Trilepton Signals in the Inert Doublet Model*. Phys. Rev. D **82** (2010) 035009, [arXiv:1005.0090 \[hep-ph\]](#).
- [22] M. Gustafsson, S. Rydbeck, L. Lopez-Honorez, and E. Lundstrom, *Status of the Inert Doublet Model and the Role of multileptons at the LHC*. Phys.Rev. **D86** (2012) 075019, [arXiv:1206.6316 \[hep-ph\]](#).
- [23] G. Belanger, B. Dumont, A. Goudelis, B. Herrmann, S. Kraml, and D. Sengupta, *Dilepton constraints in the Inert Doublet Model from Run 1 of the LHC*. Phys. Rev. **D91** (2015) no. 11, 115011, [arXiv:1503.07367 \[hep-ph\]](#).
- [24] ATLAS Collaboration, G. Aad *et al.*, *Search for direct production of charginos, neutralinos and sleptons in final states with two leptons and missing transverse momentum in pp collisions at $\sqrt{s} = 8$ TeV with the ATLAS detector*. JHEP **05** (2014) 071, [arXiv:1403.5294 \[hep-ex\]](#).
- [25] ATLAS Collaboration, M. Aaboud *et al.*, *Search for electroweak production of supersymmetric states in scenarios with compressed mass spectra at $\sqrt{s} = 13$ TeV with the ATLAS detector*. Phys. Rev. **D97** (2018) no. 5, 052010, [arXiv:1712.08119 \[hep-ex\]](#).
- [26] ATLAS Collaboration, M. Aaboud *et al.*, *Search for electroweak production of supersymmetric particles in final states with two or three leptons at $\sqrt{s} = 13$ TeV with the ATLAS detector*. [arXiv:1803.02762 \[hep-ex\]](#).
- [27] A. Goudelis, B. Herrmann, and O. Stål, *Dark matter in the Inert Doublet Model after the discovery of a Higgs-like boson at the LHC*. JHEP **09** (2013) 106, [arXiv:1303.3010 \[hep-ph\]](#).
- [28] T. Hambye, F.-S. Ling, L. Lopez Honorez, and J. Rocher, *Scalar Multiplet Dark Matter*. JHEP **0907** (2009) 090, [arXiv:0903.4010 \[hep-ph\]](#).
- [29] G. Belanger, F. Boudjema, A. Pukhov, and A. Semenov, *Dark matter direct detection rate in a generic model with micrOMEGAs 2.2*. Comput. Phys. Commun. **180** (2009) 747–767, [arXiv:0803.2360 \[hep-ph\]](#).
- [30] G. Belanger, F. Boudjema, A. Pukhov, and A. Semenov, *micrOMEGAs4.1: two dark matter candidates*. Comput. Phys. Commun. **192** (2015) 322–329, [arXiv:1407.6129 \[hep-ph\]](#).
- [31] ATLAS Collaboration, G. Aad *et al.*, *Constraints on new phenomena via Higgs boson couplings and invisible decays with the ATLAS detector*. JHEP **11** (2015) 206, [arXiv:1509.00672 \[hep-ex\]](#).
- [32] Gfitter Group Collaboration, M. Baak, J. Cuth, J. Haller, A. Hoecker, R. Kogler, K. Mönig, M. Schott, and J. Stelzer, *The global electroweak fit at NNLO and prospects for the LHC and ILC*. Eur. Phys. J. **C74** (2014) 3046, [arXiv:1407.3792 \[hep-ph\]](#).
- [33] D. Eriksson, J. Rathsmann, and O. Stal, *2HDMC: Two-Higgs-Doublet Model Calculator Physics and Manual*. Comput. Phys. Commun. **181** (2010) 189–205, [arXiv:0902.0851 \[hep-ph\]](#).
- [34] E. Lundström, M. Gustafsson, and J. Edsjö, *The Inert Doublet Model and LEP II Limits*. Phys. Rev. D **79** (2009) 035013, [arXiv:0810.3924 \[hep-ph\]](#).
- [35] DES, Fermi-LAT Collaboration, A. Albert *et al.*, *Searching for Dark Matter Annihilation in Recently Discovered Milky Way Satellites with Fermi-LAT*. [arXiv:1611.03184 \[astro-ph.HE\]](#).
- [36] XENON Collaboration, E. Aprile *et al.*, *Dark Matter Search Results from a One Tonne \times Year Exposure of XENON1T*. [arXiv:1805.12562 \[astro-ph.CO\]](#).
- [37] F. Feroz, M. P. Hobson, and M. Bridges, *MultiNest: an efficient and robust Bayesian inference tool for cosmology and particle physics*. Mon. Not. Roy. Astron. Soc. **398** (2009) 1601–1614, [arXiv:0809.3437 \[astro-ph\]](#).
- [38] F. Feroz, M. P. Hobson, E. Cameron, and A. N. Pettitt, *Importance Nested Sampling and the MultiNest Algorithm*. [arXiv:1306.2144 \[astro-ph.IM\]](#).
- [39] J. Alwall, R. Frederix, S. Frixione, V. Hirschi, F. Maltoni, O. Mattelaer, H. S. Shao, T. Stelzer, P. Torrielli, and M. Zaro, *The automated computation of tree-level and next-to-leading order differential cross sections, and their matching to parton shower simulations*. JHEP **07** (2014) 079, [arXiv:1405.0301 \[hep-ph\]](#).
- [40] K. Kohri, T. Moroi, and A. Yotsuyanagi, *Big-bang nucleosynthesis with unstable gravitino and upper bound on the reheating temperature*. Phys. Rev. **D73** (2006) 123511, [arXiv:hep-ph/0507245 \[hep-ph\]](#).
- [41] J. Pradler and F. D. Steffen, *Constraints on the Reheating Temperature in Gravitino Dark Matter Scenarios*. Phys. Lett. **B648** (2007) 224–235, [arXiv:hep-ph/0612291 \[hep-ph\]](#).
- [42] T. Moroi, H. Murayama, and M. Yamaguchi, *Cosmological constraints on the light stable gravitino*. Phys. Lett. **B303** (1993) 289–294.
- [43] M. Bolz, W. Buchmüller, and M. Plümacher, *Baryon asymmetry and dark matter*. Phys. Lett. **B443** (1998) 209–213, [arXiv:hep-ph/9809381 \[hep-ph\]](#).
- [44] M. Bolz, A. Brandenburg, and W. Buchmüller, *Thermal production of gravitinos*. Nucl. Phys. **B606** (2001) 518–544, [arXiv:hep-ph/0012052 \[hep-ph\]](#). [Erratum: Nucl. Phys. B790,336(2008)].
- [45] J. Heisig, J. Kersten, B. Panes, and T. Robens, A

- survey for low stau yields in the MSSM. JHEP **04** (2014) 053, [arXiv:1310.2825 \[hep-ph\]](#).
- [46] A. Djouadi, J.-L. Kneur, and G. Moultaka, *SuSpect: A Fortran code for the supersymmetric and Higgs particle spectrum in the MSSM*. Comput. Phys. Commun. **176** (2007) 426–455, [arXiv:hep-ph/0211331 \[hep-ph\]](#).
- [47] S. Heinemeyer, W. Hollik, and G. Weiglein, *FeynHiggs: A Program for the calculation of the masses of the neutral CP even Higgs bosons in the MSSM*. Comput. Phys. Commun. **124** (2000) 76–89, [arXiv:hep-ph/9812320 \[hep-ph\]](#).
- [48] G. Degrandi, S. Heinemeyer, W. Hollik, P. Slavich, and G. Weiglein, *Towards high precision predictions for the MSSM Higgs sector*. Eur. Phys. J. **C28** (2003) 133–143, [arXiv:hep-ph/0212020 \[hep-ph\]](#).
- [49] A. Djouadi, M. M. Muhlleitner, and M. Spira, *Decays of supersymmetric particles: The Program SUSY-HIT (SUspect-SdecaY-Hdecay-InTerface)*. Acta Phys. Polon. **B38** (2007) 635–644, [arXiv:hep-ph/0609292 \[hep-ph\]](#).
- [50] S. Kraml and D. T. Nhung, *Three-body decays of sleptons in models with non-universal Higgs masses*. JHEP **02** (2008) 061, [arXiv:0712.1986 \[hep-ph\]](#).
- [51] **HFLAV** Collaboration, Y. Amhis *et al.*, *Averages of b -hadron, c -hadron, and τ -lepton properties as of summer 2016*. Eur. Phys. J. **C77** (2017) no. 12, 895, [arXiv:1612.07233 \[hep-ex\]](#).
- [52] **LHCb** Collaboration, R. Aaij *et al.*, *Measurement of the $B_s^0 \rightarrow \mu^+\mu^-$ branching fraction and effective lifetime and search for $B^0 \rightarrow \mu^+\mu^-$ decays*. Phys. Rev. Lett. **118** (2017) no. 19, 191801, [arXiv:1703.05747 \[hep-ex\]](#).
- [53] **CMS** Collaboration, A. M. Sirunyan *et al.*, *Search for additional neutral MSSM Higgs bosons in the $\tau\tau$ final state in proton-proton collisions at $\sqrt{s} = 13$ TeV*. [arXiv:1803.06553 \[hep-ex\]](#).
- [54] K. Jedamzik, *Bounds on long-lived charged massive particles from Big Bang nucleosynthesis*. JCAP **0803** (2008) 008, [arXiv:0710.5153 \[hep-ph\]](#).
- [55] K. Jedamzik, *Big bang nucleosynthesis constraints on hadronically and electromagnetically decaying relic neutral particles*. Phys. Rev. **D74** (2006) 103509, [arXiv:hep-ph/0604251 \[hep-ph\]](#).
- [56] T. Sjostrand, S. Mrenna, and P. Z. Skands, *PYTHIA 6.4 Physics and Manual*. JHEP **0605** (2006) 026, [arXiv:hep-ph/0603175 \[hep-ph\]](#).
- [57] T. Sjöstrand, S. Ask, J. R. Christiansen, R. Corke, N. Desai, P. Ilten, S. Mrenna, S. Prestel, C. O. Rasmussen, and P. Z. Skands, *An Introduction to PYTHIA 8.2*. Comput. Phys. Commun. **191** (2015) 159–177, [arXiv:1410.3012 \[hep-ph\]](#).
- [58] W. Beenakker, R. Hopker, M. Spira, and P. M. Zerwas, *Squark and gluino production at hadron colliders*. Nucl. Phys. **B492** (1997) 51–103, [arXiv:hep-ph/9610490 \[hep-ph\]](#).
- [59] W. Beenakker, M. Krämer, T. Plehn, M. Spira, and P. M. Zerwas, *Stop production at hadron colliders*. Nucl. Phys. **B515** (1998) 3–14, [arXiv:hep-ph/9710451 \[hep-ph\]](#).
- [60] A. Kulesza and L. Motyka, *Threshold resummation for squark-antisquark and gluino-pair production at the LHC*. Phys. Rev. Lett. **102** (2009) 111802, [arXiv:0807.2405 \[hep-ph\]](#).
- [61] A. Kulesza and L. Motyka, *Soft gluon resummation for the production of gluino-gluino and squark-antisquark pairs at the LHC*. Phys. Rev. **D80** (2009) 095004, [arXiv:0905.4749 \[hep-ph\]](#).
- [62] W. Beenakker, S. Brensing, M. Krämer, A. Kulesza, E. Laenen, and I. Niessen, *Soft-gluon resummation for squark and gluino hadroproduction*. JHEP **12** (2009) 041, [arXiv:0909.4418 \[hep-ph\]](#).
- [63] W. Beenakker, S. Brensing, M. Krämer, A. Kulesza, E. Laenen, and I. Niessen, *Supersymmetric top and bottom squark production at hadron colliders*. JHEP **08** (2010) 098, [arXiv:1006.4771 \[hep-ph\]](#).
- [64] W. Beenakker, S. Brensing, M. n. Krämer, A. Kulesza, E. Laenen, L. Motyka, and I. Niessen, *Squark and Gluino Hadroproduction*. Int. J. Mod. Phys. **A26** (2011) 2637–2664, [arXiv:1105.1110 \[hep-ph\]](#).
- [65] G. Brooijmans *et al.*, “Les Houches 2017: Physics at TeV Colliders New Physics Working Group Report,” in *10th Les Houches Workshop on Physics at TeV Colliders (PhysTeV 2017) Les Houches, France, June 5-23, 2017*. [arXiv:1803.10379 \[hep-ph\]](#).